Available online at www.sciencedirect.com

ScienceDirect

Energy Procedia 77 (2015) 187 – 194

Energy Procedia

5th International Conference on Silicon Photovoltaics, SiliconPV 2015

Front-floating emitter voltage mapping of IBC Mercury cells

Pierpaolo Spinelli[a], Nicolas Guillevin[a], Teun Burgers[a] , Agnes Mewe[a], Ard Vlooswijk[b], Bart Geerligs[a], Arthur Weeber[a], Ilkay Cesar[a]

[a]*Energy Research Centre of the Netherlands (ECN), Westerduinweg 3, 1755 LE Petten, The Netherlands*
[b] *Tempress Systems BV, Radeweg 31, 8171 MD Vaassen, The Netherlands*

Abstract

Standard characterization techniques such as LBIC are difficult to apply to IBC solar cells with a front floating emitter (FFE). This is because the cells need to be under bias illumination, and this is often impossible in commercial LBIC measurement tools. To the best of our knowledge, LBIC measurements on FFE IBC cells have not been published so far. In this work we present a experimental method to spatially characterize the FFE of IBC cells and gain insights on electrical shading losses, without using LBIC. This method makes use of the commercially available CoreScan device, mapping the FFE voltage relative to the shorted back-contacts over the cell area. Using this technique we were able to resolve busbar, pads and finger features of both polarities with a scan of the front side. The scan shows that BSF features have higher voltage than emitter features, thus giving a direct evidence of the FFE pumping effect. If coupled to circuit simulation, FFE voltage maps can be the base for estimating electrical shading losses in IBC cells. The FFE voltage maps also give information on the homogeneity of the pumping effect across the wafer, e.g. affected by diffusion non-uniformity, and at least qualitatively its effect on the cell performance.

Peer review by the scientific conference committee of SiliconPV 2015 under responsibility of PSE AG

Keywords: IBC cells; front floating emitter; voltage mapping; LBIC; back-contact; n-type.

1. Mercury IBC cells at ECN

The Mercury cell developed at ECN is an interdigitated back contact (IBC) solar cell which employs a front floating emitter (FFE) instead of front surface field (FSF). While IBC cell technology has been demonstrated ideal for high-efficiency solar cells [1] due to the absence of optical shading losses from front metallization, cost effective production of these devices is still challenging. The presence of electrical shading [2] limits the choice of BSF width to less than 0.4 mm, which in turn poses severe limitations on patterning and metallization tolerances. The use of a FFE gives the IBC cell characteristics that are radically different from FSF cells [3,4]. One main feature of the FFE

Peer review by the scientific conference committee of SiliconPV 2015 under responsibility of PSE AG
doi:10.1016/j.egypro.2015.07.026

is that it enables the so called “pumping effect” that creates a lateral flow of holes in the FFE from areas above the BSF to areas above the emitter. Holes are there re-injected into the base and collected by the rear emitter [5]. This has the effect of strongly mitigating electrical shading above the BSF compared to FSF cells. Because of the pumping effect, the BSF regions can be made wider than in FSF cells without sacrificing photocurrent. This allows lower resolution processing (e.g. standard screen printing), improves manufacturability and reduces the losses due to BSF busbars. Hence, the FFE allows to widen the BSF area for busbars and pads for soldering tabs or interconnection to a conductive backsheet foil through a conductive adhesive. Such structures are illustrated in Figure 4a in Paragraph 4.

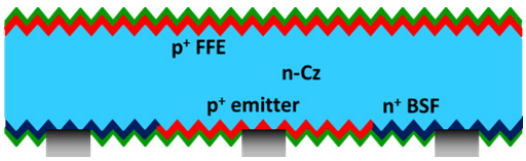

Fig. 1: schematic of a Mercury IBC solar cell with FFE.

Figure 1 shows a schematic of the Mercury cell developed at ECN. Mercury cells are processed on 6-inch semi-square n-CZ wafers using the same process tools as for our industrial n-Pasha cell process [6]. This includes diffusion of emitter and BSF regions, and screen printed metallization. Recent developments in the Mercury cell processing have resulted on 6-inch n-Cz wafers in a cell efficiency of 20.7%. In achieving these results, and also in order to further improve the efficiency, it has turned out to be important to determine the areas of the cell where losses occur. In this paper, after analyzing the limitation of standard light-beam-induced current (LBIC) techniques when applied on IBC solar cells with FFE, we present an alternative method to spatially characterize IBC solar cells with FFE. This method is based on voltage mapping using a CoreScan characterisation instrument and can be coupled to circuit simulation to study and quantify the effects on cell performance.

2. Current status of cell performance

Mercury cells of 156x156 mm^2 were processed on semi-square n-Cz wafers using the same process equipment as our industrial n-Pasha cell process [6]. Screen printed metallization was used and an isolation gap between rear emitter and BSF was omitted mainly for process simplicity. We have previously shown [7] that on small cells prepared on 6-inch substrates we obtained J_{SC} values of 41.6 mA/cm^2 for a 0.6 mm wide BSF, with a maximum efficiency of 19.4% (see Table 1). The high J_{SC} proves that bulk lifetime and front surface passivation are sufficient for near ideal current collection. Very high J_{SC} values up to 41.2 mA/cm^2 were even reached for cells with an extremely wide BSF of 1.6 mm, demonstrating the effectiveness of the Mercury concept. IV measurement on the small cells was performed by illuminating the active part of the cell between two emitter busbars but including a BSF busbar.

On 6-inch cells we obtained a cell efficiency of up to 20.7% (full size illumination) as shown in Table 1. This represents an efficiency improvement of 1.1 % absolute with respect to our previous publication [7], and was due to improvements in the process as well as in cell design. The result was obtained after process optimisation and apart from a double print of the rear metallisation no additional processing steps were introduced with respect to previously reported efficiency. Notably, a very high J_{SC} value of 41.4 mA/cm^2 was achieved on a 6-inch cell, which is on the same level as the current measured on small cells illustrating the excellent passivation behaviour of the FFE. Details of this result will be published elsewhere. The IV data were obtained with an in-house measurement conducted with a Class AAA solar simulator (Wacom), and were corrected for spectral mismatch.

Table 1. IV parameters of different Mercury cells

Cell type	Area (cm^2)	J_{SC} (mA/cm^2)	V_{OC} (mV)	FF (%)	Efficiency (%)
Small (BSF: 0.6 mm)	13	41.6	627	74.2	19.4
Small (BSF: 1.6 mm)	13	41.2	629	73.1	18.9
Previous best cell [7]	239	40.5	642	76.2	19.6
Current best cell	**239**	**41.4**	**651**	**77.0**	**20.7**

3. LBIC limitations for IBC cells with FFE

LBIC measurements of FFE IBC solar cells are difficult to obtain and have to the best of our knowledge not been published so far. This is because the cells have to be under bias illumination, in order to charge the FFE in steady state condition, and this is often unpractical in commercial LBIC measurement tools. To show this, we performed LBIC measurements by means of a Semilab WT2000 on small area IBC cells cut out from a master wafer with typical short-current densities above 41 mA/cm^2 under full area illumination. Figure 2(a) shows a schematic of the LBIC measurement. A laser light source with spot size of 100 μm is used, together with a low intensity bias light (<0.15 sun, spot size of about 1.5 mm). The laser beam and bias light are scanned over the surface of the cell and current is measured in short-circuit condition.

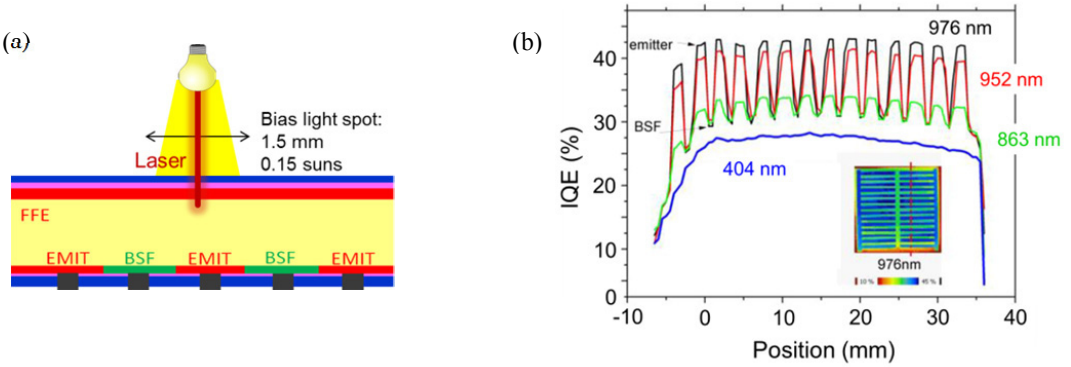

Fig. 2: (a) schematic of the LBIC measurement in the utilized Semilab tool. (b) IQE line scans as obtained by LBIC measurements.

Figure 2(b) shows four IQE line scans obtained by LBIC with different laser wavelengths. The fingers are clearly resolved by the LBIC scans for the longer wavelengths. However, the overall level of the IQE is below 50% for all wavelengths over the entire cell. This is in contrast with the IQE measured under full-area illumination, which was ~82% for a wavelength of 400 nm, as obtained by spectral response and reflection measurements. This data show that IQE response measured by LBIC using local bias light is not representative for a FFE cell under standard operation conditions (i.e. fully illuminated), and thus not directly useful for characterization of the cell losses. Full-area bias illumination is needed to obtain reliable LBIC results on FFE cells.

The low IQE at 400nm is a good estimate for the collection probability of the holes generated near the FFE crossing over to the rear emitter. This path is also followed by the holes collected by the FFE above the BSF. The collection probability is so low (~26%) because the bias light illuminates the solar cell only partially. Most of the cell is not illuminated and therefore the FFE is not charged. Being highly conductive however, the FFE is able to transport the collected holes generated in the bias light region throughout the FFE of the full cell, where holes find enough recombination centers and hence sufficient charging of the FFE-base junction is prevented. Thus these charges can never be re-injected into the base and collected by the rear emitter, resulting in low collection probabilities.

For photons absorbed above the emitter region with wavelengths that penetrate deeper into the wafer, a portion of the photogenerated charges reach the rear emitter by diffusion through the base. The closer the photons are absorbed to the rear emitter, the larger the probability to reach the emitter through this path. This is the reason for the increased IQE are longer wavelengths above the emitter. Above the BSF, however, the chance to be collected by the FFE is much larger given the geometry of the cell (150 µm thick wafer and 1200 µm wide BSF) and is nearly independent of wavelength given the large lateral distance to the emitter. Once the holes are collected, they follow the same path as the holes generated by the 400 nm wavelength light and are distributed throughout the cell. Only a small fraction of them is collected by the rear emitter. Thus the collection probability above the BSF is comparable to that of the short-wavelenghts. This also explains why the IQE of the short wavelength is no function of the rear structure. The lower IQE for 400 nm compared to the IQE at the BSF of the long wavelengths is most likely related to parasitic absorption in the SiN_x which is not accounted for in the IQE determination.

4. FFE voltage mapping using CoreScan

Here we present an alternative experimental method to spatially characterize the FFE of IBC cells. We use a CoreScan characterisation instrument [8] to map the voltage of the FFE of our IBC cell.

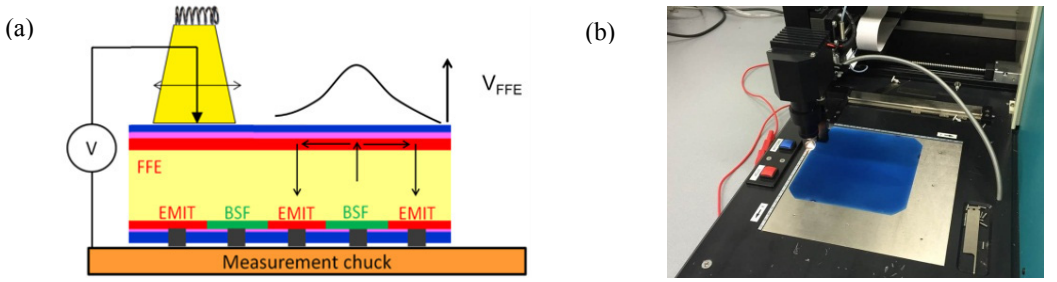

Fig. 3: (a) Schematic of the FFE voltage measurement setup. (b) Photograph of the CoreScan device used for FFE voltage measurements.

Figure 3(a) shows schematically how the FFE voltage measurement is executed. The back of the IBC cell is directly in contact with the metallic chuck, meaning that BSF and emitter polarities at the back are in short-circuit conditions. The CoreScan light source is scanned over the front side of the cell and is used to locally charge the FFE/base junction. Here, charging the FFE is more easily achieved because higher bias illumination intensities and larger spot sizes can be used in this single beam configuration with respect to the bias light LBIC measurement with a double beam configuration. The diameter of the spot is about 10 mm, with an adjustable intensity, in our case set at the maximum of about 2 suns. The FFE voltage is recorded in the center of the spot with a metal pin that scratches the front surface to contact the diffused p^+ layer. It is measured relative to the voltage of the chuck, i.e. to that of the shorted back contacts. Figure 3(b) is a photograph of the CoreScan device with a Mercury cell set for an FFE voltage scan. Note that during the measurement the lid is closed and no full-area bias light is present. This, together with the fact that the cell is under short-circuit conditions, means that the measured FFE voltage is different from that of a cell in operating conditions. Nonetheless, it is possible to study the properties of the FFE and draw conclusions about cell performances, as it will be shown in the following.

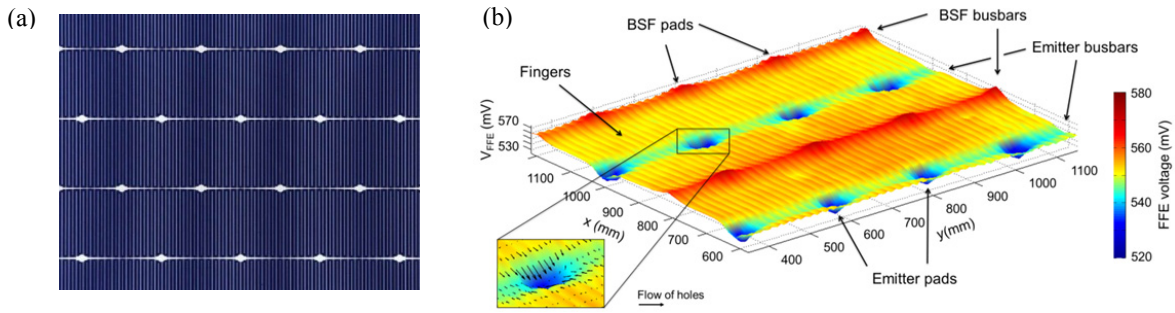

Fig. 4: (a) Photograph of the rear side of a Mercury IBC cell, showing busbar, fingers and interconnection pads. (b) 3-d representation of the FFE voltage over the cell area shown in (a). The inset shows the hole current (arrows).

Figure 4(a) shows a photograph of the rear side section of a Mercury cell. Four busbars are visible, with alternate emitter and busbar polarities (the first one from the top is a BSF busbar). The interdigitated fingers and interconnection pads [9-11] are also visible. Figure 4(b) shows the FFE voltage (vertical axis and color map) as a function of cell position (x and y axes) for the portion of the cell shown in Fig. 4(a). A clear modulation by BSF and emitter fingers, busbars and pads is observed on the voltage mapping of the FFE, despite the fact that these features are at the back side of the cell and in short-circuit conditions. The voltage is higher in the areas corresponding to BSF features, and lower in the areas corresponding to emitter features. The FFE voltage map gives information on the current flow through the front floating emitter. In fact, the majority carriers in the (p-type) FFE flow from regions of high voltage to regions of low voltage according to the relation:

$$\overrightarrow{J_h} = \sigma h \vec{\nabla} V_{FFE}$$

The inset in Fig. 4(b) shows holes current (black arrows) in the FFE as obtained from the measured data according to the formula above. The fact that a higher FFE voltage is observed over BSF regions with respect to emitter regions means that holes in the FFE are driven from the BSF areas to emitter areas. Our new measurement method thus provides a direct experimental proof of the pumping effect by the FFE.

Note that the overall average voltage of the FFE is about 550 mV, which is lower than what is expected for the p-n junction voltage under illumination (the V_{OC} of this cell was 638 mV). The lower FFE voltage can be explained by the fact that a large part of the cell is in dark conditions and carrier drift and diffusion occur towards the dark area. Furthermore, the metal pin used to probe the FFE voltage induces local damage to the FFE and thus locally increases carrier recombination.

5. Effect of base resistivity

Next we illustrate the use of the method to characterize Mercury cells. FFE voltage scans were performed on Mercury cells based on wafers featuring different base resisitivities. Figure 5 shows voltage maps of a 3 Ohm.cm (a) and a 7 Ohm.cm (b) resistivity wafer. The color scales represent the FFE voltage and is the same for both plots.

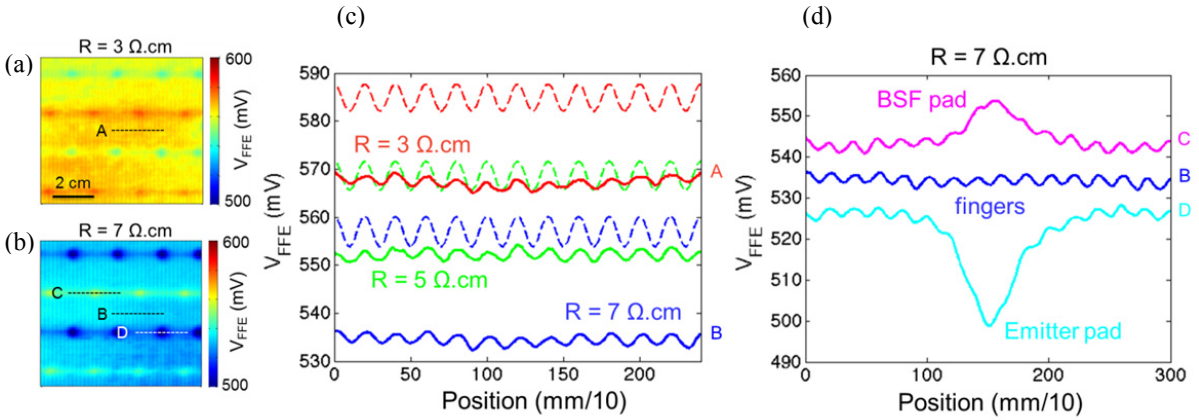

Fig. 5: FFE voltage map of a 3 Ohm.cm (a) and 5 Ohm.cm (b) base resistivity cell. (c) Measured (solid) and simulated (dashed) FFE voltage over the fingers of an IBC cell, for base resistivity of 3 Ohm.cm (red), 5 Ohm.cm (green) and 7 Ohm.cm (blue). (d) Measured FFE voltage over fingers (blue), emitter pad (light blue) and BSF pad (purple) of an IBC cell.

In each figure four busbars are visible, the first one from top being an emitter busbar. As before, other features such as fingers and pads are also recognizable. By comparing the two color maps, it is clear that the average FFE voltage value of the 3 Ohm.cm resistivity wafer is higher than of the 5 Ohm.cm wafer. Figure 5(c) shows line scans of the FFE voltage over areas with only fingers, for 3 Ohm.cm (red), 5 Ohm.cm (green) and 7 Ohm.cm (blue) base resistivity cells. Solid lines are data measured by the Corescan tool, whereas dashed lines are obtained by means of Atlas simulations [12]. Twelve unit cells are shown in the graph. The red and blue solid lines correspond to the line scans A and B shown in the color plots on the left. The average FFE voltage drops from 568 mV for the 3 Ohm.cm wafer to 552 mV for the 5 Ohm.cm wafer, down to 535 mV of the 7 Ohm.cm wafer. For each resistivity clear oscillations are observed for the FFE voltage corresponding to the fingers (emitter and BSF regions) on the rear. Interestingly, only minor variation is observed for the amplitude of the oscillation as a function of the base resistivity. As explained before, this modulation is a direct demonstration of the pumping effect by the FFE. Note that this is possible to see because the light source is large enough (~10 mm) to charge the FFE over a region corresponding to ~10 fingers.

Atlas simulations (dashed lines) show a similar trend, i.e. a reduction of the average FFE voltage when the base resistivity increases. This is due to a different built-in voltage between FFE and base. However, for all resistivities the simulated voltage is ~20 mV higher than the measured voltage. We think this difference can be explained by the fact that Atlas simulations assume full-area illuminations, whereas the measured is performed with a 1 cm light source. Thus carrier diffusion to the non-illuminated part of the cell causes a drop in the measured FFE voltage. Furthermore, the metal pin used to probe the voltage may cause carrier recombination which also lowers the voltage. Atlas simulations also confirm that the amplitude of the oscillation does not depend on the base resistivity.

Figure 5(d) shows line scans of the FFE voltage over a BSF busbar and pad region (purple), an emitter busbar and pad (light blue). A line scan over the fingers is also shown for reference (blue). These data correspond to the line C, B and D in Fig. 5(b), respectively. As can be seen the voltage over a BSF (emitter) busbar is on average higher (lower) than above the fingers. A clear peak (dip) is observed in a position corresponding to an interconnection pad. Note that the voltage scans over BSF and emitter busbar also show oscillations similar to those observed on line scans over fingers. This is due to the fact that the illumination spot is larger than the busbar width, thus carriers are generated over the finger areas next to the busbars which contribute to the creation of a modulation of the FFE voltage over the busbars.

Voltage maps can be used in combination with circuit simulations to determine the effects of the FFE voltage variation on cell performance. A detailed analysis of this method can be found in [13]. As an example, the FFE voltage drop over the emitter busbar and pads will lead to and can be correlated to a loss in cell fill-factor due to

resistive losses in the FFE. As another example, the increase of the FFE voltage over larger BSF features causes losses in the cell short-circuit current, due to electrical shading. All these effects have been quantified using circuit simulations [13].

6. Effect of inhomogeneities

Finally, voltage maps of the FFE can also be used to study the effect of FFE sheet resistance uniformity on the pumping effect. The doping process of the FFE can lead to non-uniform doping across the cell area, making the pumping effect less efficient in some regions, due to higher sheet resistance. Several methods can be used to detect doping homogeneity, such as ShereScan maps, THz absorption maps [14], etc. These techniques however do not allow to measure to what extent the FFE voltage is affected by the doping inhomogeneity. Furthermore, non-uniform surface passivation can also lead to losses in the FFE pumping effect in some areas. The FFE voltage scans presented in this work offer a possibility to gain more insights into the effect of inhomogeneities in doping or surface passivation on the FFE voltage.

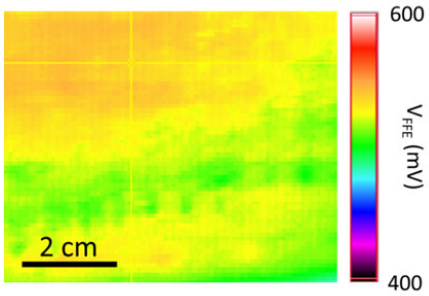

Fig. 6: FFE voltage map of an area of the cell showing a non-uniform FFE profile.

Figure 6 shows a non-uniform map of the FFE voltage of a cell area with an inhomogeneous FFE profile. An overall voltage drop is observed in some parts of the mapped area. This means that holes in the FFE are flowing towards this area of the cell and the BSF-to-emitter pumping effect is disrupted. Our technique can thus help to localize areas of the cell where the pumping effect is less effective.

7. Conclusion

We have presented a new technique to characterize IBC solar cells with FFE. This technique is based on using a well-known CoreScan device to locally probe the FFE voltage, with the cell under short-circuit condition. Using this method we were able to demonstrate voltage variations in the FFE which closely match the rear side BSF and emitter features, such as fingers, busbars and interconnection pads. A higher voltage is observed over BSF areas with respect to emitter areas, thus providing a direct proof of the pumping effect by the FFE. Other aspects such as effect of base resistivity and FFE uniformity on the FFE voltage were also studied. This technique can be combined with circuit simulation to predict the effects of voltage variations in the FFE on cell performance; it can thus be used as an alternative to standard LBIC without full-area bias illumination which is not reliable when applied on IBC cells using a FFE. Finally, we reported the current status of Mercury cell at ECN: on 6-inch wafers we reached an efficiency of 20.7%, with a high J_{SC} value of 41.4 mA/cm^2. Understanding of the variation of the operating conditions over the cell area has contributed to this result.

Acknowledgements

This work was supported by the Dutch Ministry of Economic Affairs, within the TKI framework, project IBChampion.

References

[1] Smith DD, et al. SunPower's Maxeon Gen III solar cell: high efficiency and energy yield. Proc. 39th IEEE PVSC, Tampa, 2013
[2] Hermle M, et al. Shading effects in back-junction back-contacted silicon solar cells. Proc. 33rd IEEE Photovoltaic Specialists Conference, San Diego, CA, 2008.
[3] Granek F, et al. Enhanced lateral current transport via the front N+ diffused layer of n-type high-efficiency back-junction back-contact silicon solar cells. Prog. Photovolt: Res. Appl. V17, 1 p47-56, (2009).
[4] Sah C, et al. Floating emitter solar cell. US patent 4,665,277, 1987.
[5] Cesar I, et al. Mercury: a back junction back contact front floating emitter cell with novel design for high efficiency and simplified processing, Energy Procedia 2014;55:633 – 42
[6] Romijn IG, et al. Industrial cost effective n-Pasha solar cells with >20% cell efficiency. Proc. 29th EU PVSEC, Amsterdam, 2014
[7] Cesar I, et al. Mercury: a back junction back contact front floating emitter cell with novel design for high efficiency and simplified processing. Proc. 29th EUPVSEC, Amsterdam, 2014
[8] A.S.H. van der Heide, J.H. Bultman, J. Hoornstra, A. Schönecker, Error diagnosis and optimisation of c-Si solar cell processing using contact resistances determined with the Corescanner, Solar Energy Materials & Solar Cells (Elsevier), 2002;43:p.43-.
[9] Lamers MWPE, et al. 17.9% back-contacted mc-Si cells resulting in module efficiency of 17.0%. Proc. 25th EU-PVSEC, (2010), p.1417.
[10] Guillevin N, et al. High efficiency n-type metal-wrap-through cells and modules using industrial processes, SNEC conference Shanghai, (2014).
[11] Bennett I, et al. Reducing the cost of back-contact module technology. Energy Procedia 38, 329–333 (2013)
[12] Michael S, Bates AD, and Green MS. Silvaco ATLAS as a solar cell modeling tool. 31st IEEE Photovoltaic Specialists Conference, 2005.
[13] Burgers AR, et al. Energy Procedia, this volume (2015)
[14] Nagel M, et al. THz microprobe system for contact-free high-resolution sheet resistance imaging, Proc. 28th EUPVSEC (2013)